An investigation of auroral E region energy exchange using Poker Flat Incoherent Scatter Radar observations during fall equinox conditions

Weijia Zhan[1*], Stephen R. Kaeppler[1], Miguel F. Larsen[1], Ashton Reimer[2]and Roger Varney [2]

[1]Department of Physics and Astronomy, Clemson University, Clemson, S.C. 29634-0978
[2]SRI International, Menlo Park, C.A. 94025

Key Points:

- E region energy transfer rates are estimated from PFISR measurements for the first time.
- The electromagnetic energy transfer rate and the Joule heating rate are larger in the evening sector versus the morning sector.
- Negative electromagnetic energy transfer rates occur below 110 km in the morning sector during disturbed geomagnetic conditions.

*Department of Physics and Astronomy, Clemson University, Clemson, S.C.

Corresponding author: Weijia Zhan, zweijia@clemson.edu

Abstract

We present new results using data collected by the Poker Flat Incoherent Scatter Radar (PFISR) of energy transfer rates which include the effects from neutral winds in the high latitude E-region ionosphere-thermosphere (IT) during Fall 2015. The purpose of our investigation is to understand the magnetic local time (MLT) dependence of the peak energy transfer, which occurs asymmetrically in the morning-evening (dawn-dusk) MLT sector. The statistical characteristics of both altitude-resolved and altitude-integrated energy transfer rates in the auroral E region local to PFISR during different geomagnetic conditions are quantified. Our analysis shows that the geomagnetic activity level has large impacts on the energy transfer rates. In contrast with previous investigations, we find both the altitude integrated electromagnetic (EM) energy transfer rate and Joule heating rate are larger in the evening sector than in the morning sector during all geomagnetic activity conditions. We also observe a non-negligible negative EM energy transfer rates below 110 km in the morning sector during active conditions, which is associated with neutral winds during this MLT interval. The statistical results show that the neutral winds tend to increase the Joule heating rate in a narrow altitude range in the morning sector and impact a broader region with respect to altitude and time in the evening sector in the E region under moderate and active conditions. We find that during quiet conditions that the neutral winds have a significant contribution to the Joule heating and contribute up to 75% of the Joule heating. However, during active conditions the enhanced fields are a dominant driver of Joule heating, while the neutral wind effects can reduce the Joule heating rates by 25% or more relative to the passive heating rates.

1 Introduction

The ionosphere-thermosphere (IT) at high latitudes is an important sink for magnetospheric energy input in the form of particle precipitation and Poynting flux (Thayer & Semeter, 2004). Of paramount importance is understanding the spatial and temporal distribution of energy input and dissipation through Joule heating within the IT system. The interaction of the electric fields, conductivities, and neutral winds that control the energy dissipation are complex. Even though a climatological view of Joule heating has emerged, many of the details as to how the electric fields, conductivities, and neutral winds generate the magnetic local time pattern of the Joule heating remains uncertain. This problem is further complicated by the relatively small sets of irregularly sampled data that have been collected. The purpose of this investigation is to understand the magnetic local time dependence (MLT) of the energy dissipation maxima using a nearly continuously sampled dataset of incoherent scatter radar observations.

Joule heating has been investigated globally and locally through observation and modeling, i.e., coherent and incoherent scatter radar (Banks, 1977; Thayer, 1998a; Fujii et al., 1999; Kosch & Nielsen, 1995; Kamide & Baumjohann, 1985), ground magnetometers (Kamide & Baumjohann, 1985), rockets and satellites (Cowley, 1991; Heelis & Coley, 1988; Sangalli et al., 2009), and using models (Cowley, 1991; Weimer, 2005; Zhang et al., 2005; Zhu et al., 2018). Joule heating has been shown to change the temperature and density of neutrals in the IT system (Bates, 1973; Thayer & Semeter, 2004; Wilson et al., 2006; Barth et al., 2009; Sutton et al., 2009; Barth, 2010) and to induce gravity waves that can propagate to lower latitudes (Blumen & Hendl, 1969; Brekke, 1979; Hunsucker, 1982; Sofko & Huang, 2000; Yuan et al., 2005).

Among the different observational methods used to study Joule heating, incoherent scatter radar can obtain simultaneously altitude-resolved measurements of ionospheric parameters and indirectly the neutral winds. Thus this technique is suitable for quantifying the Joule heating rates with proper accounting of the neutral wind effects, although ISRs are limited in their spatial coverage. ISR has been used to estimate the Joule heat-

ing rate in the high latitude ionosphere since the 1970s (Banks, 1977; Brekke & Rino, 1978); however, these early investigations had relatively poor range resolution.

More recent ISR investigations have quantified how neutral winds modulate Joule heating (Thayer, 1998a, 2000; Fujii et al., 1998, 1999; Aikio et al., 2012; Cai et al., 2013). Thayer (1998a) analyzed the effect of the neutral winds on the altitude-resolved Joule heating using data collected from two events observed with the Sondrestrom ISR (GeoLat:66.98°N, GMLAT: 74.2°N) during solar minimum daytime conditions. They showed that the neutral winds could lead to both enhancements and reductions of the Joule heating rate in the E region, and they showed that the E-region neutral winds caused the altitude-resolved Joule heating observations to be highly structured which accounted for the enhancements and reductions in the integrated Joule heating rates. Fujii et al. (1998) performed a case study using EISCAT (GeoLat: 69.85°N, GMLAT: 66.58°N) data at four altitudes (101, 109, 119, 132 km) and showed that the neutral wind mechanical energy transfer rate could be comparable to the Joule heating rate.

Statistical investigations of Joule heating that include the effects of the neutral winds have also been performed using observations with the Sondrestrom ISR (Thayer, 2000) and EISCAT (Fujii et al., 1999; Aikio et al., 2012; Cai et al., 2013). Thayer (2000) analyzed 95 hours of Sondrestrom ISR observations and calculated the net electrical energy input between 90–135 km. They found 59 events of enhanced EM transfer and used these events to statistically quantify the role the IT system has on modifying energy transfer. Fujii et al. (1999) examined 28 days of EISCAT CP-1 data between 1989 and 1991 to investigate the local time distribution of EM energy into Joule heating and mechanical energy at four discrete altitudes (101, 109, 119, 132 km) for different geomagnetic activity levels. More recently, Aikio et al. (2012) analyzed EISCAT observations to investigate the effects of the E region winds on the MLT variation of the altitude-integrated EM energy transfer rate and Joule heating rate using data collected from a nearly one-month experiment, 6–30 September 2005, and during a geomagnetic active interval, 11–19 November 2003. Cai et al. (2013) used the same data as Aikio et al. (2012) to investigate the altitude-resolved energy transfer rates for three different magnetic activity levels based on the Kp index.

One of the most important results from these statistical investigations was the discovery of an asymmetric energy transfer pattern with maxima in the dawn and dusk (morning and evening) MLT sectors and a minimum near magnetic midnight. However, these investigations showed significant variations in the relative strength of the maximum magnitude of energy transfer rates between the dawn and dusk sectors at different radar sites (Thayer, 2000; Fujii et al., 1999; Aikio et al., 2012). For example, Thayer (2000) showed that the dawn sector has a larger EM energy transfer rate relative to the dusk sector, although the neutral winds cause a larger reduction of the EM energy transfer rate in the dawn sector relative to the passive energy transfer rate, which is the energy deposition rate when the neutral winds are not included. Fujii et al. (1999) found that the EM energy input is equally supplied in the morning and evening sectors, but a larger Joule heating rate could either occur in the morning sector or in the evening sector depending upon the specific configuration of the neutral winds with respect to altitude. Aikio et al. (2012) showed that the integrated EM energy transfer rate is larger in the dusk sector, while the integrated Joule heating rate is larger in the morning sector due to the effects from neutral winds. Cai et al. (2013) further investigated these features using the same dataset, but using the altitude dependent results. This morning-evening asymmetry of energy transfer in the IT system is a manifestation of the asymmetric solar wind-magnetosphere coupling but it could also in turn have an impact on the magnetosphere (Walsh et al., 2014). Therefore, to have a comprehensive analysis with a large dataset will not only provide useful information about the interplay between electric field and neutral wind, but also reflect the asymmetry process in the magnetosphere-ionosphere coupling.

There remains uncertainty regarding how energy is transferred into the magnetosphere from an ionosphere-thermosphere source. Thayer (2000) reported that the net electrical energy can be transferred out of the ionosphere. However, Aikio et al. (2012) only observed electrical energy transferred out from certain altitudes in the upper E region but not in the integrated results. The altitude range that contributes to energy transfer into the magnetosphere requires further observational investigation.

Understanding the interplay between the electric fields and the neutral winds is necessary to understand how energy is transferred through Joule heating and to explain the MLT dependence of the maximum EM energy transfer rate and the Joule heating rate with respect to geomagnetic activity level. The purpose of this investigation is to present first results of E-region altitude-integrated and altitude-resolved energy transfer rates in the high latitude IT system using observations obtained with the Poker Flat Incoherent Scatter Radar (PFISR). We seek to understand the MLT dependence of the maximum EM energy transfer and the Joule heating rates, and compare our results with previous ISR studies (Fujii et al., 1999; Thayer, 2000; Aikio & Selkälä, 2009; Aikio et al., 2012; Cai et al., 2013). For this investigation, we use nearly continuously sampled 75 days of E-region measurements, that include an estimate of the E-region neutral wind, during Fall 2015 a period with geomagnetic conditions similar to previous investigations (Aikio et al., 2012; Cai et al., 2013). As in the previous investigations we quantify the energy transfer rates for different geomagnetic activity levels.

In the next section, we will introduce the radar measurements and the method used to estimate the electromagnetic energy transfer rate, the Joule heating rate, the mechanical energy transfer rate, and the passive energy deposition rate. In the Results section, we show a representative 48 hour interval of a typical measurement that was used in the statistical investigation. We then present the statistical results of the energy transfer rates as a function of MLT and geomagnetic activity level. We first present the integrated results to show the morning-evening asymmetry of the enhancements of Joule heating and EM energy transfer and then present the height resolved results to show the local effects on energy transfer rates from the neutral wind. We also present complementary observations of the electric fields, conductivities, and neutral winds and discuss our observations in the context of previous investigations. We summarize our main findings in conclusion section.

2 Measurements and methodology

2.1 PFISR measurements

PFISR is an advanced modular incoherent scatter radar (AMISR) system located at Poker Flat Research Range near Fairbanks, AK (65.13° N, 147.47°W, MLAT: 65.4° N, 0 MLT $\sim$ 11 UT). AMISR is a phased array radar capable of electronic beam steering on a pulse-to-pulse basis (Kelly & Heinselman, 2009). PFISR has been operating since late 2006 (Heinselman & Nicolls, 2008; Vadas & Nicolls, 2008) and a 4-beam low duty cycle (1%) International Polar Year (IPY) mode has been developed to make continuous climatological observations when there are no other dedicated higher duty cycle experiment modes.

The E-region neutral wind vector and electric field vector are simultaneously estimated using PFISR observations based on the algorithm described by Heinselman and Nicolls (2008). The altitude-resolved E-region neutral wind vector is determined by solving the ion momentum equation, which contains the neutral wind vector. Given the ion line-of-sight (LOS) velocities in the E- and F-region, a linear Bayesian inversion method is applied to optimally estimate the electric field vector and the altitude-resolved neutral winds. The 4-beam IPY mode has heritage with a 3-beam experiment run at the Sondrestrom incoherent scatter radar that was used to estimate the neutral winds; this

methodology is described in the review by Johnson (1990). For this investigation, we use PFISR observations that are suitable for the estimation of E-region neutral winds, which include the IPY radar mode.

Alternating codes are used to resolve the E-region ionospheric state parameters (Lehtinen et al., 1997). The PFISR experiments use a 16-baud randomized strong alternating code (e.g., Lehtinen et al., 1997) with 30 μs (4.5 km) bauds. The data are oversampled at 10 μs and processed using fractional lag processing (e.g., Huuskonen et al., 1996). For the F-region, a long-pulse experiment using a 480 or 330 μs uncoded pulse are gated to have a spacing of 36 and 24.5 km with a range resolution of 72 and 49 km, respectively.

2.2 Energy Transfer Rate

In this study, we use the definitions provided in previous investigations (e.g., Thayer, 1998a, 1998b; Cai et al., 2013) that describe the EM energy transfer rate, Joule heating rate and the mechanical energy transfer rate. The altitude-resolved EM energy transfer rate, q_{EM}, corresponds to the rate by which EM energy is transferred between the EM field and the plasma, which is given by

$$\mathbf{q_{EM}} = \mathbf{j}_\perp \cdot \mathbf{E}_\perp = \mathbf{j}_\perp \cdot \mathbf{E}^{'}_\perp + \mathbf{u_n} \cdot (\mathbf{j}_\perp \times \mathbf{B}) \tag{1}$$

where $\mathbf{j}_\perp$ is the perpendicular current density. The perpendicular electric field in the neutral wind reference frame is $\mathbf{E}^{'}_\perp$, while $\mathbf{E}_\perp$ is the electric field in the earth-fixed reference frame, where $\mathbf{E}^{'}_\perp = \mathbf{E}_\perp + \mathbf{u_n} \times \mathbf{B}$. The neutral wind is $\mathbf{u_n}$, and $\mathbf{B}$ is the Earth's magnetic field vector, which is approximately vertical downward near the pole in the northern hemisphere. In Equation 1, the first term on the right hand side, $\mathbf{j}_\perp \cdot \mathbf{E}^{'}_\perp$, is the Joule heating rate q_j, and the second term, $\mathbf{u_n} \cdot (\mathbf{j}_\perp \times \mathbf{B})$, is the mechanical energy transfer rate q_m. We can expand the Joule heating rate in the following way,

$$q_j = \mathbf{j}_\perp \cdot \mathbf{E}^{'}_\perp = \sigma_p E^{'2}_\perp = \sigma_p (\mathbf{E}_\perp + \mathbf{u_n} \times \mathbf{B})^2 \tag{2}$$

where σ_p is the Pedersen conductivity. For this investigation, we use the electron density from the vertical looking direction, which is $\sim 13^\circ$ off the field-aligned direction at the location of PFISR. The vertical beam at PFISR has better sensitivity relative to the field-aligned beam. If the IT system is treated as a passive medium, which is the case when the neutral wind is excluded, a proxy for the Joule heating rate can be defined as

$$q_j^E = \sigma_p \mathbf{E}_\perp^\mathbf{2} \tag{3}$$

which we call the passive energy deposition rate.

We can integrate Equation 2 and 3 along the magnetic field line in the E region to obtain the integrated Joule heating rate Q_j and the passive energy deposition rate Q_j^E as

$$Q_j = \int_{90}^{130} \sigma_p(z) \left[\mathbf{E}_\perp + \mathbf{u_n}(z) \times \mathbf{B}\right]^2 dz \tag{4}$$

and

$$Q_j^E = \Sigma_p^E \mathbf{E}_\perp^\mathbf{2} \tag{5}$$

where Σ_p^E is the Pedersen conductance between 90–130 km in the E region and z is the altitude. This integration range is chosen because the uncertainty is larger in the neutral wind estimation at higher E region altitude (Thayer, 1998a). The integrated me-

chanical energy transfer rate and EM energy transfer rate are,

$$Q_m = \int_{90}^{130} \mathbf{u_n}(z) \cdot (\mathbf{j}_\perp \times \mathbf{B}) dz \tag{6}$$

and

$$Q_{EM} = Q_j + Q_m, \tag{7}$$

respectively.

All the vectors are in a local geomagnetic coordinate system with x, y, z as east, north, and anti-parallel directions, respectively (Heinselman & Nicolls, 2008). From the equations above, Q_j and Q_j^E are positive definite while Q_m and Q_{EM} could be signed either positive or negative. Positive Q_m indicates that the neutral winds obtain energy from the plasma, while negative Q_m indicates that the neutral wind is doing work on the plasma. Similarly, positive Q_{EM} indicates that EM energy is dissipated in the ionosphere-thermosphere, i.e., the IT system is an energy sink, while negative Q_{EM} indicates that the ionosphere is an energy source (Thayer & Vickrey, 1992; Thayer, 1998b; Aikio et al., 2012).

For this investigation, σ_p is calculated using Equation 2.40(a) in Kelley (2009) and the ion-neutral collision frequencies used are equation 4.88 and expressions in Table 4.5 of Schunk and Nagy (2009). These equations are not repeated here for brevity. The neutral densities used to calculate the collision frequency are obtained from the NRL-MSISE00 model (Picone et al., 2002). We use the International Geomagnetic Reference Field (IGRF) model to estimate $\mathbf{B}$ (Thébault et al., 2015).

The current density is calculated using ISR observations in the same way as equation 8 in (Thayer, 1998a) using the following formulas,

$$\mathbf{j}_\perp = en_e(\mathbf{V}_{\perp i} - \mathbf{V}_{\perp e}) = en_e(V_x + \frac{E_y}{B})\hat{\mathbf{x}} + en_e(V_y - \frac{E_x}{B})\hat{\mathbf{y}} \tag{8}$$

where e is the elementary electron charge and n_e is the E-region electron density, provided by the alternating code observations. The ion drift perpendicular to the magnetic field, $\mathbf{V}_{\perp i} = V_x\hat{\mathbf{x}} + V_y\hat{\mathbf{y}}$, is estimated from the LOS velocities using the methodology described in Heinselman and Nicolls (2008). The electrons remain coupled to the magnetic field down to 80 km and still drift in the $\mathbf{E}\times\mathbf{B}$ direction (Brekke, 2013; Richmond & Thayer, 2000). Therefore, for the perpendicular electron drifts, $\mathbf{V}_{\perp e} = \mathbf{E} \times \mathbf{B}/\mathbf{B^2}$, is a good approximation in the E-region, and we use the electric field $\mathbf{E}$ estimated from the F-region long pulse observations. Then the electric field is used to calculate the passive energy deposition rate q_j^E using equation 3. The Joule heating q_j can be obtained through equation 2. The Mechanical energy transfer rate q_m is obtained by using $\mathbf{u_n} \cdot (\mathbf{j}_\perp \times \mathbf{B})$ and the EM energy transfer rate q_{EM} is obtained by adding up q_j and q_m. The approach taken differs from Thayer (1998a). We have made a comparison of both approaches, shown in the supporting information S1, and obtained similar results in an average sense. A more detailed investigation will be pursued to explore the occasions when the two techniques differ to identify what properties of the ISR measurements produce such results.

2.3 PFISR Observations

For this study, we use a subset of data from the larger database of PFISR observations spanning the period from 2010-2019. The dataset is mainly composed of IPY mode data, however other higher duty cycle radar modes are also used when the measurements are suitable for the calculation of Joule heating. We select high quality measurements using a threshold of SNR $\geq$ -20 dB. The electric fields, neutral winds and energy transfer rates are derived using equations described in Section 2.2. We use a data analysis routine that combines data from multiple beam directions instead of using a single verti-

cal beam under the assumption that the velocity vectors are homogeneous in the radar field of view (fov) (Zou et al., 2009). Also, the small scale latitudinal variation of the electron density in the radar fov in the E region, if it exists, is not considered in this study.

The PFISR observations cover the E-region between 90 km–130 km with an altitude resolution of 5 km. A running median filter with a 1-hour window is applied at a time step of 15 minutes to all the derived parameters (i.e., conductivities, electric fields, neutral winds, energy transfer rates). For the statistical results, the median will decrease the impact of outliers (Press et al., 2007). Given our choice of resolution, there are 96 elements for the time array and 9 elements for the altitude array.

In this study, we use the regional SuperMAG Auroral Electrojet, SME, index (hereafter referred to as SMEr) as a proxy for geomagnetic activity levels. There are a few reasons why we use this geomagnetic index instead of AE or KP. First, the SMEr index is derived using many more magnetometer stations with greater global coverage (Gjerloev, 2012; Newell & Gjerloev, 2011, 2014) than KP and AE. Second, Joule heating enhancements are mainly a local phenomenon (Thayer, 2000) and SMEr accounts for the local-time variation of the auroral electrojet. The dataset is then divided into three groups according to the SMEr index: quiet (0,100), moderate (100,200), and high (200+), respectively.

To enable a similar comparison of our results with previous investigations (e.g., Aikio et al., 2012; Cai et al., 2013), we used measurements from Fall (September, October and November) 2015. The solar and geomagnetic activity levels in Fall 2015 were similar to Fall 2003 and 2005, when the measurements from the EISCAT investigations were obtained (Aikio et al., 2012; Cai et al., 2013). In both studies, the mean AP and mean F10.7 were 16 and 107, respectively.

3 Results

3.1 September 17-18, 2015 Event

We first present a typical example of PFISR observations that covers both quiet and disturbed conditions during September 17-18, 2015. This two day interval shows an example of typical events that are used in the statistical investigation and the data quality associated with the PFISR observations.

Figure 1(a) shows the variation of SMEr during the observation interval. For comparison, the variation of the AE index is plotted during the same interval. The green and black markers on the upper region of Figure 1(a) indicate the intervals corresponding to the IPY mode and higher duty cycle modes of the radar, respectively. Figure 1(b) shows the electron density. Figure 1(c) and 1(d) present the altitude-resolved zonal and meridional winds, respectively. The zonal and meridional electric fields are shown in Figure 1(e) as blue and red, respectively. Positive values of zonal and meridional wind and electric field components are geomagnetic eastward and northward, respectively. The altitude-resolved passive energy deposition rate (q_j^E), Joule heating rate (q_j), mechanical energy transfer rate (q_m), and EM energy transfer rate (q_{EM}) are presented in Figure 1(f)-(i), respectively. The black contour lines in Figure 1(h) and Figure 1(i) correspond to the dividing line between positive and negative. The four integrated energy transfer rates are presented in Figure 1(j).

In Figure 1(a), SMEr (blue) indicates two disturbed periods during the first and second evenings while AE (red) shows additional disturbed periods in the afternoon sector during the two days. From the typical daytime electron density shown in Figure 1(b), SMEr is a better proxy for localized auroral activity. In Figure 1(b), typical daytime E-region electron density profiles are observed. Auroral precipitation is observed during the disturbed periods indicated by SMEr.

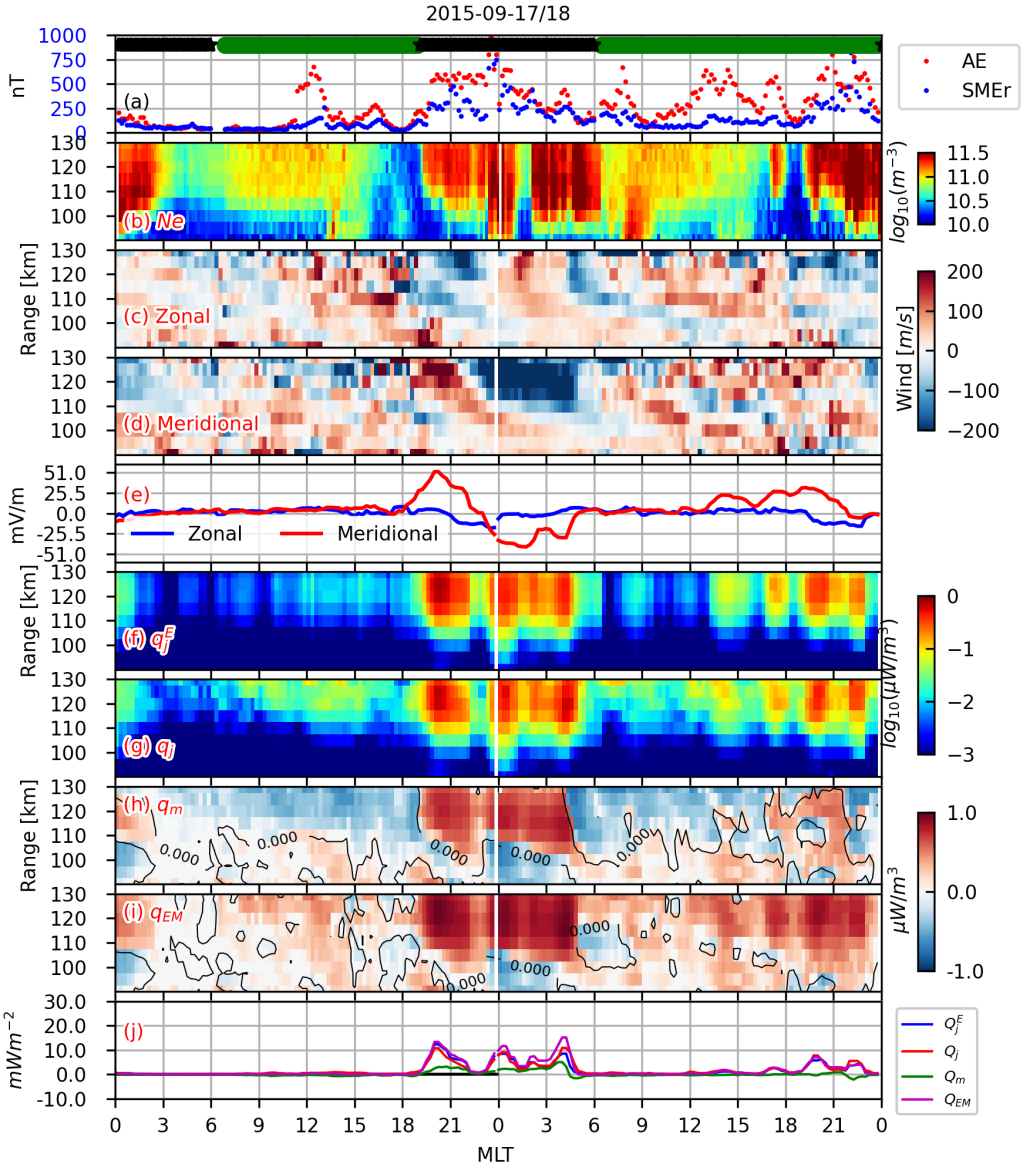

Figure 1. PFISR observation on September 17-18, 2015 (0000 MLT ∼ 1100 UT). (a) AE index (red dots) and SMEr (blue dots), green and black markers on the top indicate low duty cycle (IPY) and higher duty modes of PFISR, respectively; (b) electron density N_e; (c) and (d) zonal and meridional winds; (e) zonal (blue) and meridional (red) electric fields; (f) and (g) $log_{10}(q_j^E)$ and $log_{10}(q_j)$; (h) and (i) q_m and q_{EM}, the black contour lines represent 0; (j) Q_j^E (blue), Q_j (red), Q_m (green) and Q_{EM} (magenta).

In Figure 1(c) and 1(d), the wind data are noisy when the radar is operating in the IPY mode, specifically between 0600-1800 MLT on September 17 and between 0600-2400 MLT on September 18. This relatively noisy data is attributed to the low duty cycle of the IPY mode, along with modest electron densities, i.e., low backscatter. However, an enhanced pattern of neutral winds is observed when the radar is operated in high duty cycle modes between 0000-0600 MLT and 1800-0600 MLT. In Figure 1(e), the zonal electric field is small with a magnitude near zero but becomes westward in the evening sector on both days. Enhanced northward electric fields are observed in the evening sectors on both days and enhanced southward electric fields are observed in the morning sector on September 18. The strong meridional electric field is a signature of the two-cell plasma convection pattern.

In Figure 1(f), strong enhancements ($\sim 1\mu W/m^3$) of the passive energy deposition rate q_j^E are observed when the electric field is large. A moderate enhancement ($\sim 0.03\mu W/m^3$) of q_j^E is observed when the electric field is small between 0000-0100 MLT on September 17 and between 0800-0900MLT on September 18. In Figure 1(g), enhancements of the Joule heating rate, q_j, are observed in the MLT sectors when q_j^E is enhanced; Joule heating rate enhancements ($\sim 0.1\mu W/m^3$) are also observed during the daytime between 0900-1600 MLT on September 17 and September 18 when the electric field is small. These observations show that the neutral winds generate Joule heating during daytime when the electric field is small and that the electric field has a dominant role in generating Joule heating during the nightside MLT sector.

Figure 1(h) shows enhancements ($\sim 0.5\mu W/m^3$) of the mechanical energy transfer rate q_m that are mainly positive throughout the night of September 17, which suggests that the neutral winds obtain mechanical energy from the plasma during this period. During the daytime, the mechanical energy transfer rate is mainly negative ($\sim -0.3\mu W/m^3$) above 110 km and modestly positive ($\sim 0.2\mu W/m^3$) below 110 km. In addition, negative values ($\sim -0.3\mu W/m^3$) of q_m also appear in the lower E region below 110 km in the morning sector between 0000-0300 MLT during the two-day interval.

In Figure 1(i), the EM energy transfer rate, q_{EM}, is largely enhanced ($\sim 1\mu W/m^3$) throughout the night on September 17, moderately enhanced ($\sim 0.5\mu W/m^3$) in the evening sector on September 18, and is mostly positive at all altitudes during daytime, although with modest magnitudes ($\sim 0.2\mu W/m^3$). These signatures suggest that EM energy is transferred into the plasma. Between 0000-0300 MLT below 110 km altitude, negative values ($\sim -0.2\mu W/m^3$) of q_{EM} occur. This feature of negative EM energy transfer is commonly observed in the lower E region in the morning sector.

Figure 1(j) shows that enhancements ($\sim 11mW/m^2$, $\sim 10mW/m^2$, $\sim 15mW/m^2$) of the integrated terms, Q_j^E (blue), Q_j (red) and Q_{EM} (magenta) appear mainly during the intervals when the electric field is enhanced. Q_m (green) is positive ($2-4mW/m^2$) throughout the night of 17 September and in the second evening sector except in short intervals (0400-0500 MLT and 2200-2300 MLT on September 18). As mentioned above, these intervals of positive Q_m correspond to energy that is transferred to the neutral winds from the plasma. This example indicates that the altitude resolved mechanical energy transfer rate can be highly structured while the integrated results are small.

3.2 Statistical Results for Fall 2015

In this section, we present the statistical results of the altitude-integrated energy transfer rates and then present the results of altitude-resolved energy transfer rates in Fall 2015. All the results are shown in Figure 2, with additional supporting information found in Figure 3.

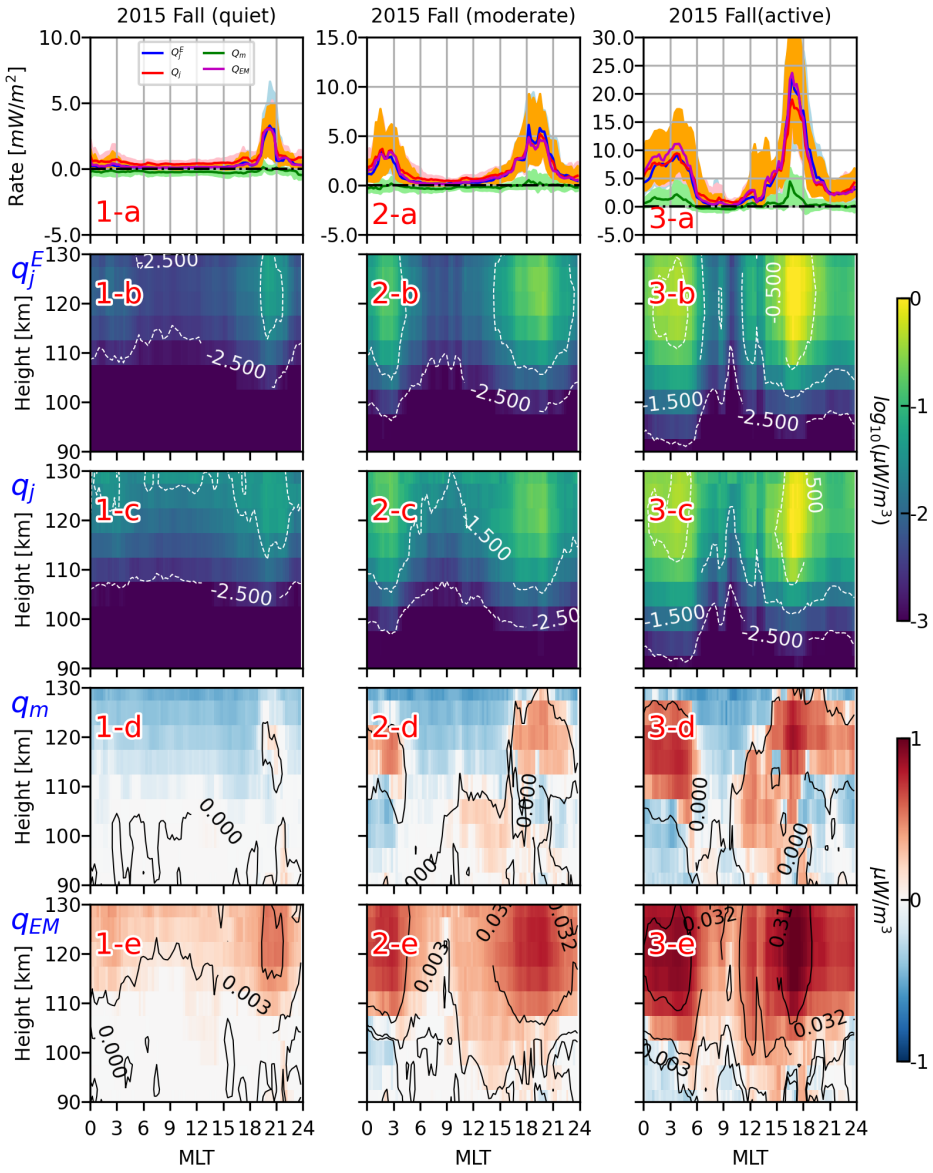

Figure 2. Energy transfer rates from top to bottom: (a) integrated energy transfer rates (Q_j^E (blue), Q_j (red), Q_m (green) and Q_{EM} (magenta)), (b) altitude-resolved passive energy deposition rate q_j^E; (c) altitude-resolved Joule heating rate q_j; (d) mechanical energy transfer rate q_m and (e) EM energy transfer rate q_{EM} under quiet (1st column), moderate (2nd column) and active (3rd column) conditions in Fall 2015. q_j^E and q_j are plotted on a logarithmic scale while q_m and q_{EM} are plotted on a linear scale.

3.2.1 Integrated Energy Transfer Rates

The first row of Figure 2 presents the variations of the median integrated energy transfer rates Q_j^E, Q_j, Q_m and Q_{EM} as a function of magnetic local time (MLT) as blue, red, green and magenta curves, respectively. The corresponding light blue, pink, light green and orange shaded regions are the bounds of the first and third quartiles. The remaining four rows show the altitude-resolved parameters, q_j^E, q_j, q_m and q_{EM}. The columns from left to right correspond to quiet (SMEr $<$ 100 nT), moderate (100 nT $\leq$ SMEr $<$ 200 nT), and active conditions (SMEr $\geq$ 200 nT) in Fall 2015. The relative percentage of measurements correspond to 60%, 20% and 20% for quiet, moderate, and active conditions, respectively. Note the different scales on the vertical axes in the first row.

During quiet conditions, Figure 2(1-a) shows that the integrated Joule heating, EM energy transfer and passive energy deposition rates, Q_j, Q_{EM} and Q_j^E, are small with magnitudes less than 1 mW/m^2 in most of the MLT sectors, except between 1900-2300 MLT in the evening sector. With the exception of the evening MLT interval, the net Joule heating is mainly due to the mechanical energy which is driven by the neutral winds, while the net EM energy transfer from the magnetosphere is very small. In the evening sector, between 1900-2300 MLT, enhancements of Q_j, Q_{EM} and Q_j^E are observed with a maximum magnitude of ~ 3 mW/m^2, while Q_m increases in magnitude between 2000-2100 MLT. These observations suggest that the EM energy transfer rate is the result of the convection electric field in the evening sector during quiet conditions.

Under moderate conditions, Figure 2(2-a) shows enhanced Q_j, Q_j^E and Q_{EM} in the morning and evening sectors. The peak values of Q_j, Q_j^E and Q_{EM} in the morning and evening sectors are roughly a factor of two larger than quiet conditions. The larger peaks in the evening sector indicate an asymmetry of the energy transfer rate relative to the morning sector. The morning-evening asymmetry of the energy transfer rate under disturbed conditions has also been reported in previous ISR investigations but the MLT of the peak magnitudes vary within these studies as mentioned in the Introduction (Thayer, 2000; Fujii et al., 1999; Aikio et al., 2012). This asymmetry will be discussed in detail in the fourth section. Finally, the integrated mechanical energy transfer rate, Q_m, is negative and increases to near zero for a short period in the morning and evening sectors. The magnitudes are much smaller than that of Q_j, Q_j^E and Q_{EM}, especially during the morning and evening sectors. This indicates that the net effects of mechanical energy transfer on Joule heating is modest during moderately disturbed condition.

During active conditions, in Figure 2(3-a), there are much stronger enhancements of Q_j, Q_j^E and Q_{EM} observed in the morning and evening sectors. The peak median magnitudes are more than three times larger during active conditions relative to moderate conditions. Similar to moderate condition, a morning-evening asymmetry is observed with larger magnitudes of the Joule heating and EM energy transfer rates in the evening sector. However, in contrast to quiet and moderate conditions, positive values of the mechanical energy transfer rate, Q_m, appear both in the morning and evening sectors and the maximum median magnitude in the evening sector is around 5 mW/m^2. This indicates that the neutral winds obtain mechanical energy in both the morning and evening sectors with longer temporal extent in the evening sector. Thayer (2000) found that the neutral winds obtain mechanical energy both in the morning and evening sectors, but the effects of neutral winds are greater in the morning sector than in the evening sector. In Aikio et al. (2012), the net effect of the neutral winds in the morning sector is only to provide mechanical energy to the plasma.

Our investigation is limited to the E-region energy transfer rates between 90-130 km. We restricted our neutral wind estimation to altitudes below 130 km because the motion of the ions above 130 km are more strongly tied to the $\mathbf{E}\times\mathbf{B}$ direction versus the neutral wind (Sangalli et al., 2009; Burchill et al., 2012). Therefore the estimation of the neutral winds using LOS ion velocities above this altitude is highly uncertain. The

only energy transfer rate we can estimate above 130 km without reliable neutral wind estimates is the passive energy dissipation rate, and section 4.4 discusses the extra passive Joule heating above 130 km. This restriction limits our ability to make direct comparisons to other studies that use different altitude extents, such as Aikio et al. (2012) who study 80-180 km.

3.2.2 Altitude-Resolved Energy Transfer Rates

Figure 2 presents the median altitude-resolved passive energy deposition rate and the Joule heating rate, q_j^E and q_j, in the second (Figure 2-b) and third (Figure 2-c) rows on a logarithmic scale, respectively. The mechanical energy transfer rate and EM energy transfer rate, q_j^m and q_{EM}, as shown in the fourth (Figure 2-d) and fifth (Figure 2-e) rows on a linear scale, respectively. Contour lines of energy transfer rates are also included in Figure 2-b, Figure 2-c and Figure 2-e. Contour lines in row Figure 2-d represent the division between positive and negative values.

To aide in our analysis of the energy transfer rates, we also present the following quantities in Figure 3: the median Pedersen 3(A) and Hall 3(B) conductivities, the median zonal 3(C) and meridional 3(D) neutral winds, and the median zonal 3(E) and meridional 3(F) electric fields. The three columns correspond to quiet, moderate and active conditions, respectively.

The results for quiet condition are presented in the left column of Figure 2. In Figure 2(1-b) and 2(1-c), there are small enhancements ($0.058\mu W/m^3, 0.059\mu W/m^3$) of q_j^E and q_j mainly in the upper E region between 110 – 130 km in the evening MLT sector. The enhancement of q_j^E occurs when the meridional electric field is large in the evening sector, as shown in Figure 3(F). In addition, in Figure 3(A), the median Pedersen conductivity between 110 – 130 km from 1800 – 2100 MLT is smaller than in other MLT sectors. Therefore, the enhancement of the passive energy deposition rate is primarily driven by the large meridional electric field associated with the dusk plasma convection cell.

Figure 2(1-d) shows that the mechanical energy transfer rate q_m is modest with a value near zero in the lower E region and negative ($-0.015\mu W/m^3$) in the upper E region. These observations of the mechanical energy rate are consistent with the statistical result during quiet conditions (Kp <= 2+) found by Cai et al. (2013). They reported that q_m is near zero in the lower E region, but becomes negative in the higher E-region altitudes in most of the MLT sectors. The mechanical energy transfer rate is weakly positive around 2100 MLT in the evening sector mainly between 110 – 120 km.

The EM energy transfer rate, q_{EM} in Figure 2(1-e) shows a distribution in upper E-region in the morning and evening sectors similar to the Joule heating rate, q_j^E, but with minor differences. The main difference appears in the upper E region during the daytime, when q_{EM} is smaller relative to q_j^E. This indicates that the EM energy that originates from the magnetosphere is reduced due to the presence of the neutral winds by altering the current in such a way as to reduce the current component in the electric filed direction (Thayer, 1998a).

Figure 2(2-b) and Figure 2(2-c) show that q_j^E and q_j are enhanced ($0.29\mu W/m^3, 0.24\mu W/m^3$) in the morning and evening sectors during moderate conditions. The enhancements in both sectors extend to lower altitudes and have a longer duration in time relative to quiet conditions. The peak in the evening sector shifts to earlier MLT between 1800–1900 MLT compared to quiet condition. The morning-evening asymmetry of the energy transfer rates is also evident; we find a stronger enhancement in the evening sector relative to the morning sector. The large passive energy deposition rate is caused by the enhanced meridional electric field in the evening sector, while the Pedersen conductivity is small in this MLT sector as shown in Figure 3A. In the morning sector, enhancements of the passive

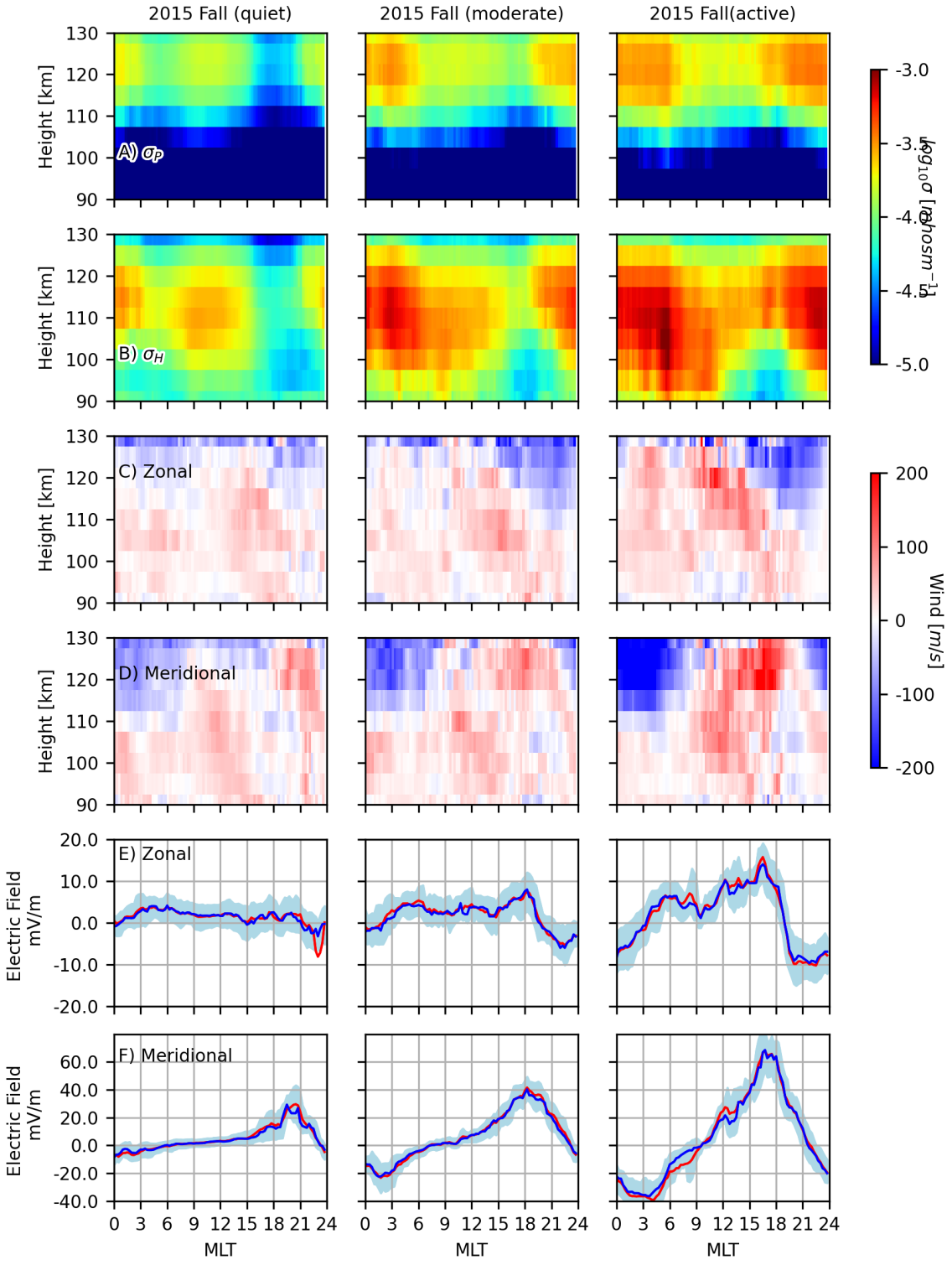

Figure 3. From top to bottom, the median values are shown of the: (A) Pedersen conductivity; (B) Hall conductivity; (C) zonal neutral winds (positive: eastward); (D) meridional winds (positive: northward); (e) zonal electric field (positive: eastward) and (F) meridional electric field (positive: northward) under quiet (left), moderate (middle) and active (right) conditions in Fall 2015. In E and F, blue (red) curves correspond to median (mean) electric fields. Shaded areas indicate 1st and 3rd quartiles respect to medians.

energy deposition rate are caused by both the enhanced electric field and Pedersen conductivity as shown in Figure 3.

Figure 2(2-d) shows the behavior of the mechanical energy transfer, q_m. There are three regions with positive values ($< 0.04\mu W/m^3$) of q_m: between 110 – 120 km from 0000-0600 MLT, below 110 km between 0900-2100 MLT, and between 110 – 130 km from 1500-2400 MLT. Positive q_m appears in a broader region with respect to time and altitude in the evening sector. Negative values ($> -0.065\mu W/m^3$) of q_m also appear in three time intervals: between 90 – 110 km and above 120 km in the morning sector, above 110 km during daytime and between 95 – 110 km in the evening sector. These results show that the integrated mechanical energy transfer rates are small in magnitude while the altitudinal variation is highly structured.

Figure 2(2-e) shows that the total electromagnetic energy transfer rate, q_{EM}, again has a similar distribution to the Joule heating rate q_j^E above 110 km. The main difference appears in the lower E region, especially in the morning sector between 0000-0300 MLT when non-negligible negative EM energy transfer rate appears ($> -0.013\mu W/m^3$), indicating that EM energy could be generated locally due to the presences of neutral winds.

During active conditions, Figure 2(3-b) and Figure 2(3-c) show much larger enhancements ($1.36\mu W/m^3, 1.25\mu W/m^3$) of q_j^E and q_j in broader regions with respect to time and altitude in the morning (0000-0600 MLT) and evening (1500-2100 MLT)sectors compared to moderate conditions. The magnitudes of both rates in the evening sector are much larger than in the morning sector. In Figure 2 (3-d) and Figure 2(3-e), larger enhancements ($0.30\mu W/m^3, 1.50\mu W/m^3$) in the morning and evening sectors are also observed in q_m and q_{EM}. In addition, the mechanical energy transfer rates during daytime are also enhanced. This indicates that the differences of these parameter between moderate and active conditions exist mainly in the magnitude of the response. We also observe that the peak MLT of the energy transfer rates moves nearer to noon, which is similar to results reported by Aikio et al. (2012) and Cai et al. (2013).

We summarize the following key results from the measurements at Poker Flat:

1. Two maxima in the morning and evening sectors and a minimum around midnight of the energy transfer are observed under moderate and active conditions. We observe that the energy transfer rates in the evening sector are larger than in the morning sector.
2. The geomagnetic activity shows large positive impact on the enhanced energy transfer. This impact not only appears in the integrated results but also in the altitude-resolved results. Enhanced positive (in the higher E region) and negative (in the lower E region) mechanical energy transfer rates are observed in the morning and evening sectors under active condition (Figure 2(3-d)). The large negative mechanical energy transfer rates below 100 km in the morning sector even lead to negative EM energy transfer rates (Figure 2(3-e)).
3. Consistent with previous observations, we see in Figure 2 that as the geomagnetic activity level increases, the peak energy transfer rates move toward local noon.

4 Discussion

In this section, we explain how the interplay between the conductivities, electric fields, and neutral winds provide a first order explanation of the MLT dependence of the electromagnetic energy transfer rate and Joule heating described above over Poker Flat. We first examine the impact of the neutral winds through a simple theoretical analysis to determine whether neutral winds are a source or sink at different altitudes and MLT sectors in the E region. We will then discuss the differences we found in our observations relative to previous ISR investigations (Aikio et al., 2012; Cai et al., 2013; Fujii et al.,

1999; Thayer, 2000). In addition, to present the extent of the effects of neutral winds on Joule heating, we quantify the difference between the passive energy deposition rate, q_j^E, and the Joule heating rate, q_j, normalized to q_j. Finally, an estimation of the passive energy transfer rate above 130 km, where the uncertainty of neutral wind estimation is large, is presented.

4.1 Theoretical Analysis of the Effects of Neutral Wind

To understand how the neutral winds affect the Joule heating rate during different MLT sectors, we performed a derivation invoking the following assumptions. First, the upper E region is dominated by the Pedersen conductivity and the lower E region is dominated by the Hall conductivity (Brekke, 2013); this result is also supported by Figure 3. Second, the zonal electric field is negligible compared to the meridional electric field according to our measurements (Figures 3E and 3F) and the results shown in Aikio et al. (2012).

We use a geomagnetic coordinate system with the x axis in the zonal direction, the y axis in the meridional direction and the z axis in the vertical direction. The unit vectors along x, y and z are $\hat{\mathbf{x}}, \hat{\mathbf{y}}, \hat{\mathbf{z}}$, respectively. As $q_m = \mathbf{U_n} \cdot (\mathbf{j}_\perp \times \mathbf{B})$ and $\mathbf{j}_\perp = \sigma_\mathbf{P}\mathbf{E}_\perp + \sigma_\mathbf{H}\mathbf{b} \times \mathbf{E}_\perp$ (Aikio et al., 2012), we have $\mathbf{U_n} = U_x\hat{\mathbf{x}} + U_y\hat{\mathbf{y}}$, $\mathbf{E}_\perp = E_x\hat{\mathbf{x}} + E_y\hat{\mathbf{y}}$ and $\mathbf{B} = -B\hat{\mathbf{z}}$ in the northern hemisphere assuming that the vertical components of neutral wind and electric field are negligible and that only the vertical component of geomagnetic field matters. Then,

$$\begin{aligned} q_m &= \mathbf{U_n} \cdot ((\sigma_\mathbf{P}\mathbf{E}_\perp + \sigma_\mathbf{H}\mathbf{b} \times \mathbf{E}_\perp) \times \mathbf{B}) \\ &= B(E_x(\sigma_P U_y + \sigma_H U_x) + E_y(\sigma_H U_y - \sigma_P U_x)) \end{aligned} \tag{9}$$

From this expression, q_m is mainly modulated by the altitude dependent conductivities and neutral winds. As Figure 3 shows, the magnitudes of the zonal electric field are typically smaller than the meridional electric field, especially in the morning and evening sectors during disturbed conditions. If we assume that $|E_x| << |E_y|$, then equation 9 simplifies to

$$q_m \approx BE_y(-\sigma_P U_x + \sigma_H U_y) \tag{10}$$

As evident in Figures 3E and 3F, E_y is mainly positive in the evening sector and negative in the morning sector. Based on this fact and the assumptions above, we can determine the sign of q_m through Equation 10 in the following way: in the morning sector, the sign of q_m is determined by the sign of U_x in the upper E region and by the sign of $-U_y$ in the lower E region; in the evening sector, the sign of q_m is determined by $-U_x$ in the upper E region and by U_y in the lower E region.

Now, we can infer whether the neutral wind is a source or sink of energy in the E region. In Figure 3 under active conditions in the morning sector, the eastward wind between 110 and 125 km implies that q_m is positive and the neutral wind is a sink of energy at these altitudes. The northward wind in the lower E region, < 110 km, implies that q_m is negative in this region. In the evening sector, the westward wind above 110 km implies that q_m is positive and the southward wind between 90 and 110 km indicates that q_m is negative. In addition, since in the afternoon sector, the electric field is primarily meridional, then for a northward wind in the lower E region implies q_m is positive. These results are consistent with the behavior of the mechanical energy transfer rate shown above in Figure 2.

4.2 Comparison with Previous Studies

In the results section, we showed that the PFISR observations have different features relative to previous ISR investigations. We now discuss possible causes for these differences. The measurements used in this study are from one radar site (PFISR), and therefore the results and conclusions are most applicable to the region local to PFISR.

To make suitable comparisons of our results with other ISR studies we consider possible differences caused by the different geomagnetic and geographic locations of the radar sites. The relative locations of PFISR (GeoLat: 65.13°N, GMLAT: 65.4°N), ESICAT (GeoLat: 69.85°N, GMLAT: 66.58°N) and Sondrestrom (GeoLat:66.98°N, GMLAT: 74.2°N) ISRs are presented in Figure 4 with the auroral boundaries at 4 different universal times (UTs) during moderately disturbed conditions (Kp = 3) during a typical day in Fall 2015 obtained with the statistical Feldstein-Starkov auroral oval model (Sigernes et al., 2011; Starkov, 1994). During this day, PFISR and EISCAT are located in the auroral oval in the dark hemisphere, and are located in subauroral region during sunlit hours. The small difference in geomagnetic latitudes ensure that the two radars sample the similar region in the auroral oval. Therefore, it is likely that forcing from the magnetosphere is similar at this two radar sites. Aikio et al. (2012) determined through the variation of height integrated conductances that the region illuminated by the EISCAT radars are in the auroral oval mainly from the dusk to midnight sector and dawn sector and in the subauroral region during the daytime. We assume that PFISR observations are from a similar sampling region and we expect to see some consistent features between our observations and those from EISCAT. In addition, Sondrestrom is located at much higher geomagnetic latitude but at a similar geographic latitude with respect to PFISR. Sondrestrom samples the polar cap or poleward auroral boundary during nighttime and the auroral oval during daytime (Thayer, 1998a). This could enable us to find the potential geomagnetic latitudinal dependence of the energy transfer between PFISR and Sondrestrom (Thayer, 2000).

There are two significant differences between our observations compared with the other ISR investigations. The first difference is the MLT dependence of maximum Joule heating rate. Previous statistical studies (Thayer, 2000; Fujii et al., 1999; Aikio et al., 2012; Cai et al., 2013) reported two local maxima in the morning and evening sectors of the EM energy transfer rate and the Joule heating rate. However, the relative magnitudes of these two maxima are different among the earlier studies. Our results show that the median EM energy transfer rate and the median Joule heating rate are both larger in the evening sector. This larger enhancement of the EM energy transfer rate is mainly due to the larger enhancement of the meridional electric field in the evening sector. In addition, due to the small net mechanical energy transfer rate, the Joule heating rate is still larger in the evening sector. The high latitude ionosphere in the morning and evening sectors are more electric field driven (Thayer, 2000, and references therein), so the maxima in these two regions are largely determined by the variation of the electric field. In this study and in that of Aikio et al. (2012), the meridional electric field in the evening sector is larger than in the morning sector, thus leading to a larger EM energy transfer rate in the evening sector in both studies. However, the integrated energy transfer rate results in Aikio et al. (2012) show larger enhancement of the Joule heating rate in the morning sector than in the evening sector, which is the opposite of our results. One key difference is the mechanical energy transfer rate. The magnitude of Q_m in Aikio et al. (2012) shows stronger enhancements in the morning and evening sectors relative to our results. In Thayer (2000), the authors found the dawnside electric field is larger than in the dusk sector during enhanced energy transfer events; this observation could explain the larger EM energy transfer rate in the morning sector in his study.

The Joule heating rates show different characteristics due to the influence of the neutral wind. During active conditions, Thayer (2000) found a reduction of EM energy transfer by neutral winds both in the dawn and dusk sectors, which is similar to our re-

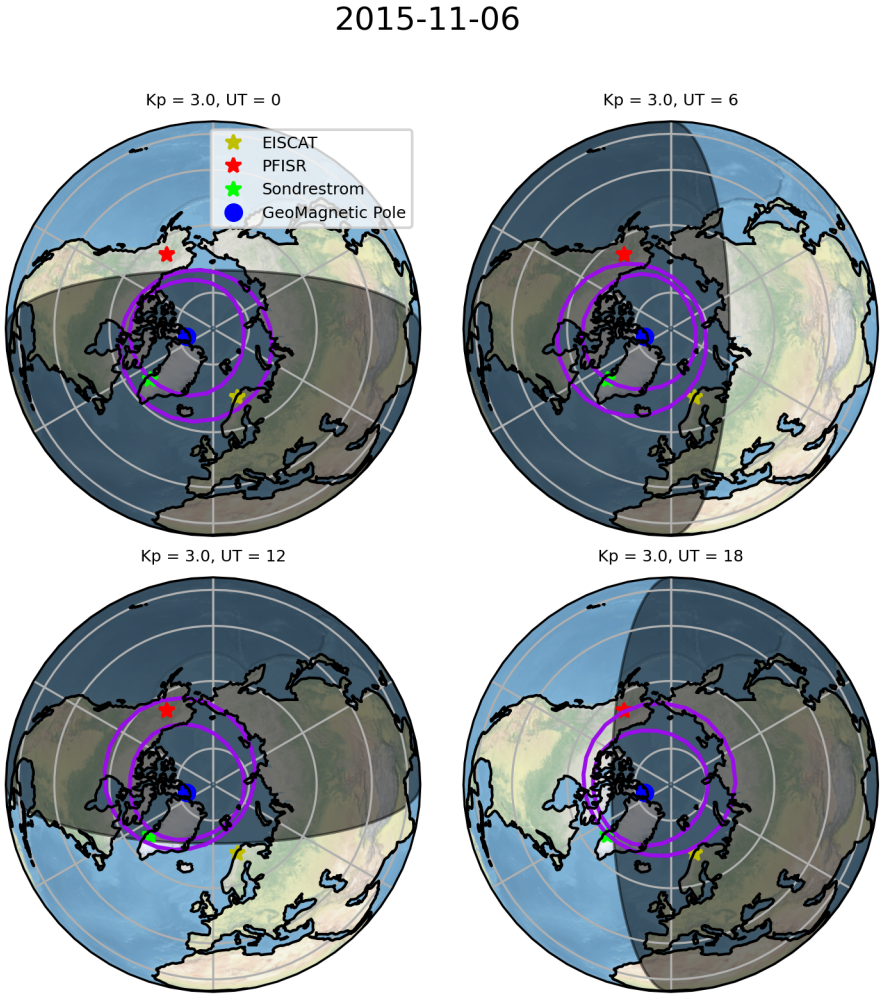

Figure 4. Geographic locations of PFISR (red star), EISCAT Tromoso (yellow star) and Sondrestrom (green star) on November 6, 2015 at 4 different UT with Kp = 3. The auroral boundaries (purple) are obtained through the Feldstein-Starkov oval model (Sigernes et al., 2011; Starkov, 1994). The dark hemisphere is plotted in shaded gray region and the geomagnetic pole is labeled in blue.

sults. However, (Aikio et al., 2012) showed that the neutral winds tend to decrease Joule heating rates in the evening sector, but increase the Joule heating rate in the morning sector. Although the larger Joule heating rates in the morning sector can be attributed to the contribution from the neutral wind above 145 km, which is outside of our integration range (90-130 km) and the range used in the investigation by Thayer (2000) (90-135 km).

The second difference is the altitudes of negative EM energy transfer rate under active conditions. Our results show negative EM energy transfer rates mainly below 110 km in the morning sectors. Negative EM energy transfer rates are not reported in the results by Cai et al. (2013) but are shown in the lower quartile profile above 140 km during active conditions in the evening sector. This difference comes from the stronger negative mechanical energy transfer rate below 110 km in the morning sector in our data set, which is caused by the larger neutral wind in the lower E region. In Figure 3C and Figure 3D, the magnitude of the meridional wind below 110 km in the morning sector is approximately 50 m/s, while Cai et al. (2013) found that the neutral wind at lower altitudes are near zero. Thayer (2000) also showed negative integrated EM energy transfer rates but did not specify the time and altitudes.

The geographic and geomagnetic locations of the ISRs have different contributions to the terms in the Joule heating equations. The geographic location of the ISRs is important for understanding the conductivity structure due to solar illumination and neutral wind structure, particularly from lower atmospheric sources. The geomagnetic locations of the ISRs can result in differences in auroral-activity driven conductivities and the convection electric field, depending on how the ISRs sample the auroral oval. The auroral produced electron density enhancements can strongly impact the conductivity and strong electric field during disturbed intervals can lead to significant enhancements of Joule heating. Geomagnetic versus geographic differences in Joule heating rates could be investigated during an interval when ISR observations were collected simultaneously over at least a diurnal cycle; however, such an investigation is outside the scope of this study.

4.3 Quantifying the Effects of Neutral Winds

While the previous section presented the statistical features of the mechanical energy transfer rate and the Joule heating rate in the presence of the neutral winds, this section will analyze to what extent the neutral winds impact the Joule heating rate in a statistical sense. The difference between the passive energy deposition rate and the Joule heating rate has been investigated in Thayer (1998a) to emphasize the change of the Joule heating rate with and without the effects of the neutral wind; we note that this definition is different than the ratio used in the investigation by Thayer (2000). We define the percent difference between the median passive energy deposition rate, q_j^E, and the median Joule heating rate, q_j normalized to the Joule heating rate. This ratio can be expressed as

$$\begin{aligned} r &= \frac{q_j^E - q_j}{q_j} \times 100\% \\ R &= \frac{Q_j^E - Q_j}{Q_j} \times 100\% \end{aligned} \tag{11}$$

with r, R the height-resolved and integrated terms, respectively. When r and R are negative, it means the neutral wind tends to increase the Joule heating rate, and when r and R are positive, the neutral wind decreases the Joule heating. A value of zero means that the Joule heating rate is driven by the electric field, while a value of -100% corresponds

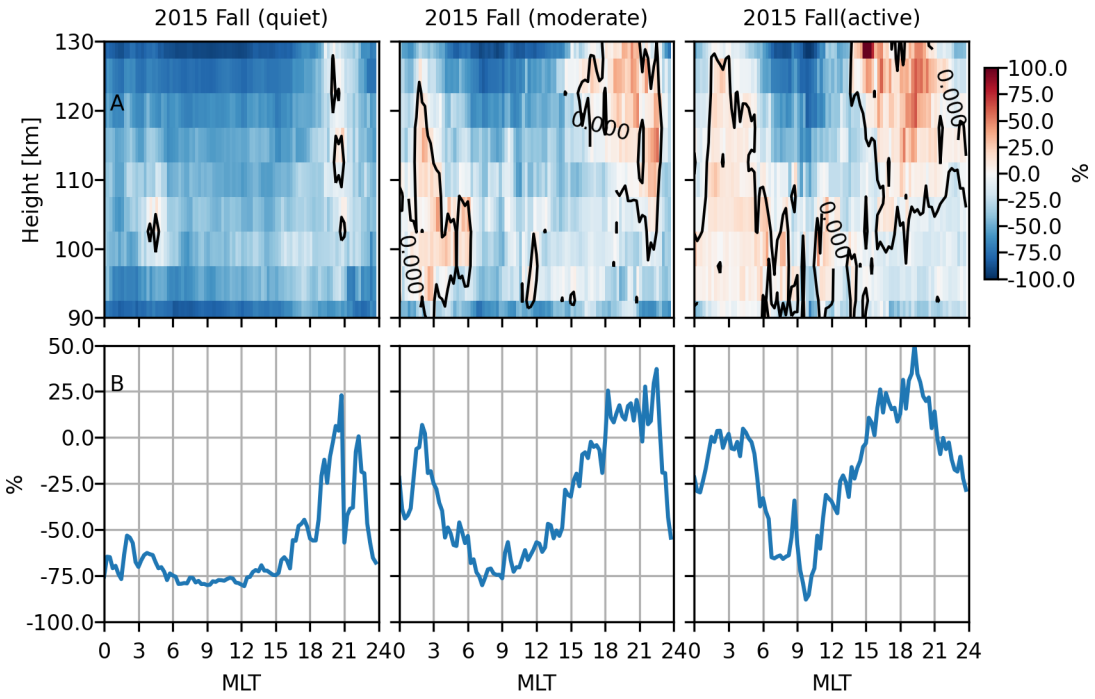

Figure 5. Percent difference between the passive energy dissipation rate and Joule heating rate, normalized to Joule heating rate.

to a contribution only from the neutral wind. Since the passive energy deposition rate is always positive, r and R are always greater than or equal to -100%.

The medians are presented in Figure 5. The first and second row show r and R, respectively. From left to right, the columns show the results during quiet, moderate and active conditions, respectively. From the first row, we find that the regions with positive r in the morning and evening sectors that becomes broader in altitude extent as the geomagnetic activity level increases. From the second row, we see that with the increase of geomagnetic activity level in the morning sector (0000-0600 MLT), R increases from -75%- -50%, to -50%- 0% and to around 0 ; during daytime (0600-1500 MLT), R increases from around -75% , to -25% - -75% and to -75% - 0; during evening sector (1500 - 2400 MLT), R increases from -50% - 25%, to -25% - 25% and to 0 - 50%.

The observations during moderate and active conditions indicate that in the morning the net effect of the neutral winds on the Joule heating is small. In the evening sector, neutral winds reduce the energy dissipation at most altitudes. However, the neutral winds increase the Joule heating rate below 100 km.

4.4 Additional Joule heating above 130 km

As mentioned above, the assumptions associated with the neutral wind estimation break down above $\sim$ 130 km altitude. However, the Pedersen conductivity peaks near 125 km (Richmond & Thayer, 2000; Brekke, 2013) and has considerably large magnitudes above 125 km. Therefore, the integration range limits could lead to an underestimation of the integrated Joule heating rate in this study. We quantify the magnitude that the Joule heating rate could be underestimated above 130 km in the following way.

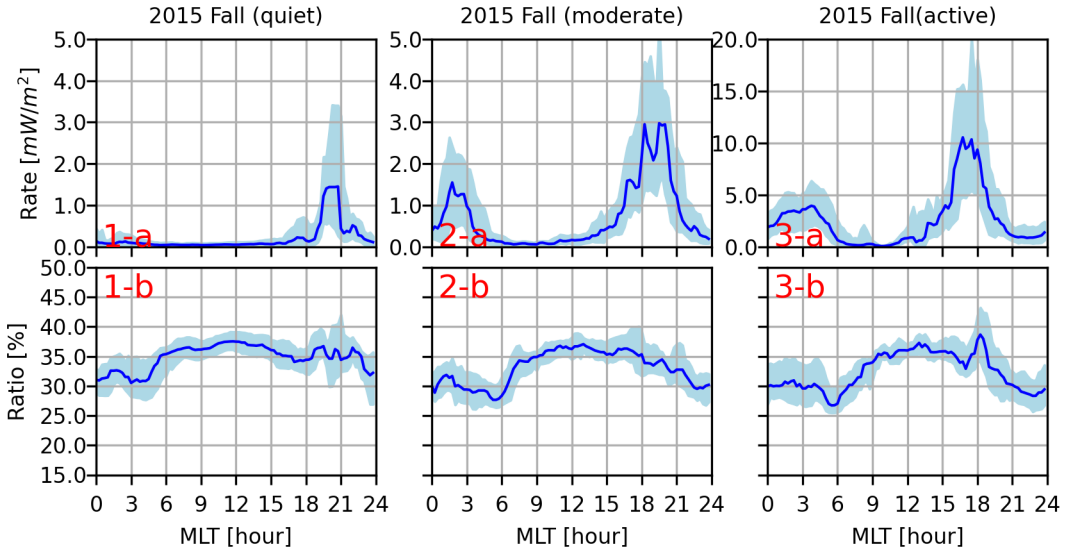

Figure 6. The integrated passive energy deposition rate above 130 km (top) and the percentage difference normalized to integrated passive energy deposition rate between 90-150 km (bottom) during quiet (left), moderate (middle), and active (right) conditions. Thick lines indicate median values and the upper and lower quartiles are shown by a shaded color.

We estimate the integrated passive energy deposition rate Q_j^E above 130 which is shown in Figure 6(a). Figure 6(b) shows the percent difference between the integrated passive heating rate over 130-150 km and the total integrated passive heating rate between 90-150 km.

From Figure 6(a), the variation of the median value of the underestimated Q_j^E varies along a similar pattern with the maxima in the morning and evening sectors as shown in Figure 2(a) but with smaller magnitudes. The largest value varies from around 1.5 mW/m^2 during quiet condition, to 3 mW/m^2 during moderate condition, and to 10 mW/m^2 during active condition. From Figure 6(b), the relative underestimation in percentage varies between 30%-38% during quiet condition, to between 28%-38% during moderate condition, and to between 27%-39% during active condition. This percentage difference of the underestimated Joule heating rate is slightly larger during daytime relative to nighttime and relatively consistent during different geomagnetic conditions.

5 Conclusion

This paper presents a comprehensive study of the characteristics of energy transfer rates using nearly 1400 hours of Poker Flat Incoherent Scatter Radar observations covering different geomagnetic conditions in Fall 2015. The purpose of this investigation is to quantify the MLT dependence of the Joule heating and EM energy transfer rate above Poker Flat. The nearly continuously sampled measurements from PFISR have confirmed that there are two maxima of the enhanced energy transfer rates in the morning and evening sectors and that the geomagnetic activity has a positive impact on these enhancements, which is consistent with previous studies at other radar sites, such as EISCAT (Fujii et al., 1999; Aikio et al., 2012) and Sondrestrom (Thayer, 2000). However, our observations have shown two major differences that have not been previously reported.

The first difference is that our observations show larger enhancements of EM energy transfer and Joule heating both in the evening sector, which is in contrast to previous investigations (Thayer, 2000; Fujii et al., 1999; Aikio et al., 2012; Cai et al., 2013). A detailed comparison of the MLT dependence of the maximum Joule heating rate and EM energy transfer rate have shown that these enhancements are larger in the evening sector relative to the morning sector due to the larger meridional electric field at the latitude of PFISR in the evening sector. This asymmetry of the meridional electric field can be further associated with the asymmetry of the two-cell convection pattern and processes that drive the asymmetry of the two-cell convection pattern (Walsh et al., 2014). Our comparison combined with the altitude resolved distribution of mechanical energy transfer rates also suggest the local effects on energy transfer caused by neutral winds (Thayer, 1998a; Cai et al., 2013).

The second difference is that we observed an interval with negative EM energy transfer rates below 110 km between 0000-0300 in the morning sector under disturbed condition, which is not shown in previous investigations. These negative EM energy transfer rates are associated with the neutral winds during this interval. The neutral wind in lower E region in the morning sector are similar to winds reported in earlier chemical release experiments (Larsen et al., 1989; Brinkman et al., 1995; Larsen et al., 1995). Our observations underline the local effects on energy transfer caused by the neutral wind.

In addition, we quantified the contribution of the neutral wind to Joule heating and found that as much as 75% of the Joule heating comes from the neutral wind associated mechanical energy transfer under quiet condition and that more than 25% reduction of the Joule heating is associated with the neutral wind during active conditions.

Finally, we also estimated the additional passive energy deposition rate above 130 km. The additional passive energy deposition rate could be between 30-40% of the total passive energy deposition rate between 90-150 km. The percent difference does not vary significantly as a function of MLT for constant geomagnetic activity.

Acknowledgments

The raw data of PFISR measurements used in this study can be obtained from the Madrigal database (https://isr.sri.com/madrigal). The processed data of neutral winds, electric fields, conductivities and energy transfer rates can be obtained from this repository (https://doi.org/10.5281/zenodo.4627540). WZ and SRK were supported by National Science Foundation AGS–1853408 and AGS–1552269. MFL was supported by the National Science Foundation AGS–2012994. This material is based upon work supported by the Poker Flat Incoherent Scatter Radar which is a major facility funded by the National Science Foundation through cooperative agreement AGS–1840962 to SRI International. We gratefully acknowledge the SuperMAG collaborators (`https://supermag.jhuapl.edu/info/?page=acknowledgement`).

References

Aikio, A. T., Cai, L., & Nygrén, T. (2012). Statistical distribution of height-integrated energy exchange rates in the ionosphere. *Journal of Geophysical Research: Space Physics*, *117*(10), 1–14. doi: 10.1029/2012JA018078

Aikio, A. T., & Selkälä, A. (2009). Statistical properties of Joule heating rate, electric field and conductances at high latitudes. *Annales Geophysicae*, *27*(7), 2661–2673. doi: 10.5194/angeo-27-2661-2009

Banks, P. (1977, feb). Observations of joule and particle heating in the auroral zone. *Journal of Atmospheric and Terrestrial Physics*, *39*(2), 179–193. doi: 10.1016/0021-9169(77)90112-X

Barth, C. A. (2010). Joule heating and nitric oxide in the thermosphere,

738 2. *Journal of Geophysical Research: Space Physics*, *115*(A10). doi:
739 10.1029/2010JA015565
740 Barth, C. A., Lu, G., & Roble, R. G. (2009). Joule heating and nitric oxide in the
741 thermosphere. *Journal of Geophysical Research: Space Physics*, *114*(5), 1–9.
742 doi: 10.1029/2008JA013765
743 Bates, H. F. (1973). Atmospheric expansion through Joule heating by horizontal
744 electric fields. *Planet. Space Sci.*, *21*(12). doi: 10.1016/0032-0633(73)90184-0
745 Blumen, W., & Hendl, R. G. (1969, mar). On the Role of Joule Heating as a Source
746 of Gravity-Wave Energy above 100 km. *J. Atmos. Sci.*, *26*(2), 210–217. doi: 10
747 .1175/1520-0469(1969)026⟨0210:OTROJH⟩2.0.CO;2
748 Brekke, A. (1979). On the relative importance of Joule heating and the Lorentz
749 force in generating atmospheric gravity waves and infrasound waves in
750 the auroral electrojets. *J. Atmos. Terr. Phys.*, *41*(5), 475–479. doi:
751 10.1016/0021-9169(79)90072-2
752 Brekke, A. (2013). *Physics of the Upper Polar Atmosphere* (Vol. 58) (No. 12).
753 Berlin, Heidelberg: Springer Berlin Heidelberg. doi: 10.1007/978-3-642-27401
754 -5
755 Brekke, A., & Rino, C. L. (1978). High-resolution altitude profiles of the auroral
756 zone energy dissipation due to ionospheric currents. *Journal of Geophysical Re-*
757 *search: Space Physics*, *83*(A6), 2517-2524. doi: 10.1029/JA083iA06p02517
758 Brinkman, D. G., Walterscheid, R. L., Lyons, L. R., Kayser, D. C., Christensen,
759 A. B., Sharber, J. R., ... Larsen, M. F. (1995). E Region neutral winds in
760 the postmidnight diffuse aurora during the atmospheric response in Aurora 1
761 Rocket Campaign . *Journal of Geophysical Research*, *100*(A9), 17309. doi:
762 10.1029/94ja02814
763 Burchill, J. K., Clemmons, J. H., Knudsen, D. J., Larsen, M., Nicolls, M. J., Pfaff,
764 R. F., ... Sangalli, L. (2012). High-latitude e region ionosphere-thermosphere
765 coupling: A comparative study using in situ and incoherent scatter radar ob-
766 servations. *Journal of Geophysical Research: Space Physics*, *117*(2), 1–11. doi:
767 10.1029/2011JA017175
768 Cai, L., Aikio, A. T., & Nygrén, T. (2013). Height-dependent energy exchange
769 rates in the high-latitude e region ionosphere. *Journal of Geophysical Research:*
770 *Space Physics*, *118*(11), 7369–7383. doi: 10.1002/2013JA019195
771 Cowley, S. W. H. (1991, March). Acceleration and heating of space plasmas: con-
772 cepts. *Annales Geophysicae*, *9*, 176-187.
773 Fujii, R., Nozawa, S., Buchert, S. C., & Brekke, A. (1999). Statistical charac-
774 teristics of electromagnetic energy transfer between the magnetosphere, the
775 ionosphere, and the thermosphere. *Journal of Geophysical Research: Space*
776 *Physics*, *104*(A2), 2357–2365. doi: 10.1029/98ja02750
777 Fujii, R., Nozawa, S., Matuura, N., & Brekke, A. (1998). Study on neutral wind con-
778 tribution to the electrodynamics in the polar ionosphere using EISCAT CP-1
779 data. *Journal of Geophysical Research: Space Physics*, *103*(A7), 14731–14739.
780 doi: 10.1029/97ja03687
781 Gjerloev, J. W. (2012). The SuperMAG data processing technique. *J. Geophys. Res.*
782 *Sp. Phys.*, *117*(9), 2018. doi: 10.1029/2012JA017683
783 Heelis, R. A., & Coley, W. R. (1988). Global and local Joule heating effects seen by
784 DE 2. *J. Geophys. Res.*, *93*(A7), 7551. doi: 10.1029/ja093ia07p07551
785 Heinselman, C. J., & Nicolls, M. J. (2008). A Bayesian approach to electric
786 field and E -region neutral wind estimation with the Poker Flat Advanced
787 Modular Incoherent Scatter Radar . *Radio Science*, *43*, RS5013. doi:
788 10.1029/2007rs003805
789 Hunsucker, R. D. (1982). Atmospheric gravity waves generated in the high-latitude
790 ionosphere: A review. *Reviews of Geophysics*, *20*(2), 293-315. doi: 10.1029/
791 RG020i002p00293
792 Huuskonen, A., Lehtinen, M. S., & Pirttilä, J. (1996). Fractional lags in alternat-

ing codes: Improving incoherent scatter measurements by using lag estimates at noninteger multiples of baud length. *Radio Science*, *31*(2), 245-261. doi: 10.1029/95RS03157

Johnson, R. M. (1990). Lower-thermospheric neutral winds at high latitude determined from incoherent scatter measurements - A review of techniques and observations. *Advances in Space Research*, *10*, 261-275. doi: 10.1016/0273-1177(90)90259-3

Kamide, Y., & Baumjohann, W. (1985). Estimation of electric fields and currents from international magnetospheric study magnetometer data for the cdaw 6 intervals: Implications for substorm dynamics. *Journal of Geophysical Research: Space Physics*, *90*(A2), 1305-1317. doi: 10.1029/JA090iA02p01305

Kelley, M. C. (2009). *The Earth ' s Ionosphere Second Edition.*

Kelly, J. D., & Heinselman, C. J. (2009). Initial results from Poker Flat Incoherent Scatter Radar (PFISR). *J. Atmos. Solar-Terrestrial Phys.*, *71*(6-7), 635. doi: 10.1016/j.jastp.2009.01.009

Kosch, M. J., & Nielsen, E. (1995). Coherent radar estimates of average high-latitude ionospheric joule heating. *Journal of Geophysical Research: Space Physics*, *100*(A7), 12201-12215. doi: 10.1029/95JA00821

Larsen, M. F., Marshall, T. R., Mikkelsen, I. S., Emery, B. A., Christensen, A., Kayser, D., ... Walterscheid, R. (1995). Atmospheric Response in Aurora experiment: Observations of E and F region neutral winds in a region of post-midnight diffuse aurora. *Journal of Geophysical Research*, *100*(A9), 17299. doi: 10.1029/95JA01346

Larsen, M. F., Mikkelsen, I. S., Meriwether, J. W., Niciejewski, R., & Vickery, K. (1989). Simultaneous observations of neutral winds and electric fields at spaced locations in the dawn auroral oval. *J. Geophys. Res.*, *94*(A12), 17235. Retrieved from `http://doi.wiley.com/10.1029/JA094iA12p17235` doi: 10.1029/JA094iA12p17235

Lehtinen, M. S., Huuskonen, A., & Markkanen, M. (1997). Randomization of alternating codes: Improving incoherent scatter measurements by reducing correlations of gated autocorrelation function estimates. *Radio Science*, *32*(6), 2271-2282. doi: 10.1029/97RS02556

Newell, P. T., & Gjerloev, J. W. (2011). Evaluation of supermag auroral electrojet indices as indicators of substorms and auroral power. *Journal of Geophysical Research: Space Physics*, *116*(A12). doi: 10.1029/2011JA016779

Newell, P. T., & Gjerloev, J. W. (2014). Local geomagnetic indices and the prediction of auroral power. *Journal of Geophysical Research: Space Physics*, *119*(12), 9790-9803. doi: 10.1002/2014JA020524

Picone, J. M., Hedin, A. E., Drob, D. P., & Aikin, A. C. (2002, dec). NRLMSISE-00 empirical model of the atmosphere: Statistical comparisons and scientific issues. *Journal of Geophysical Research: Space Physics*, *107*(A12), 1648. doi: 10.1029/2002JA009430

Press, W., Teukolsky, S., Vetterling, W., & Flannery, B. (2007). *Numerical recipes 3rd edition: The art of scientific computing.* Cambridge University Press.

Richmond, A. D., & Thayer, J. P. (2000). Ionospheric electrodynamics: A tutorial. In *Magnetospheric current systems* (p. 131-146). American Geophysical Union (AGU). doi: 10.1029/GM118p0131

Sangalli, L., Knudsen, D. J., Larsen, M. F., Zhan, T., Pfaff, R. F., & Rowland, D. (2009). Rocket-based measurements of ion velocity, neutral wind, and electric field in the collisional transition region of the auroral ionosphere. *Journal of Geophysical Research: Space Physics*, *114*(4), 1–10. doi: 10.1029/2008JA013757

Schunk, R., & Nagy, A. (2009). *Ionospheres: Physics, Plasma Physics, and Chemistry.* Cambridge: Cambridge University Press. doi: 10.1017/CBO9780511635342

Sigernes, F., Dyrland, M., Brekke, P., Chernouss, S., Lorentzen, D. A., Oksavik, K., & Deehr, C. S. (2011, oct). Two methods to forecast auroral displays. *J. Sp. Weather Sp. Clim.*, *1*(1), A03. doi: 10.1051/swsc/2011003

Sofko, G. J., & Huang, C.-S. (2000). Superdarn observations of medium-scale gravity wave pairs generated by joule heating in the auroral zone. *Geophysical Research Letters*, *27*(4), 485-488. doi: 10.1029/1999GL003692

Starkov, G. (1994). Mathematical model of the auroral boundaries. *GEOMAGNETISM AND AERONOMY C/C OF GEOMAGNETIZM I AERONOMIIA*, *34*, 331–336.

Sutton, E. K., Forbes, J. M., & Knipp, D. J. (2009). Rapid response of the thermosphere to variations in joule heating. *Journal of Geophysical Research: Space Physics*, *114*(A4). doi: 10.1029/2008JA013667

Thayer, J. P. (1998a, jan). Height-resolved Joule heating rates in the high-latitude E region and the influence of neutral winds. *Journal of Geophysical Research: Space Physics*, *103*(A1), 471–487. doi: 10.1029/97JA02536

Thayer, J. P. (1998b). Radar measurements of the electromagnetic energy rates associated with the dynamic ionospheric load/generator. *Geophysical Research Letters*, *25*(4), 469–472. doi: 10.1029/97GL03660

Thayer, J. P. (2000). High-latitude currents and their energy exchange with the ionosphere-thermosphere system. *Journal of Geophysical Research: Space Physics*, *105*(A10), 23015–23024. doi: 10.1029/1999ja000409

Thayer, J. P., & Semeter, J. (2004). The convergence of magnetospheric energy flux in the polar atmosphere. *Journal of Atmospheric and Solar-Terrestrial Physics*, *66*(10), 807–824. doi: 10.1016/j.jastp.2004.01.035

Thayer, J. P., & Vickrey, J. F. (1992). On the contribution of the thermospheric neutral wind to high-latitude energetics. *Geophysical Research Letters*, *19*(3), 265–268. doi: 10.1029/91GL02868

Thébault, E., Finlay, C. C., Beggan, C. D., Alken, P., Aubert, J., Barrois, O., ... Zvereva, T. (2015). International geomagnetic reference field: The 12th generation international geomagnetic reference field - The twelfth generation. *Earth, Planets Sp.*, *67*(1). doi: 10.1186/s40623-015-0228-9

Vadas, S. L., & Nicolls, M. J. (2008, jan). Using PFISR measurements and gravity wave dissipative theory to determine the neutral, background thermospheric winds. *Geophysical Research Letters*, *35*(2), L02105. doi: 10.1029/2007GL031522

Walsh, A. P., Haaland, S., Forsyth, C., Keesee, A. M., Kissinger, J., Li, K., ... Taylor, M. G. G. T. (2014, jul). Dawn–dusk asymmetries in the coupled solar wind–magnetosphere–ionosphere system: a review. *Annales Geophysicae*, *32*(7), 705–737. doi: 10.5194/angeo-32-705-2014

Weimer, D. R. (2005). Improved ionospheric electrodynamic models and application to calculating Joule heating rates. *J. Geophys. Res.*, *110*(A5), A05306. doi: 10.1029/2004JA010884

Wilson, G. R., Weimer, D. R., Wise, J. O., & Marcos, F. A. (2006). Response of the thermosphere to joule heating and particle precipitation. *Journal of Geophysical Research: Space Physics*, *111*(A10). doi: 10.1029/2005JA011274

Yuan, Z., Fujii, R., Nozawa, S., & Ogawa, Y. (2005). Statistical height-dependent relative importance of the Lorentz force and Joule heating in generating atmospheric gravity waves in the auroral electrojets. *J. Geophys. Res.*, *110*(A12), A12303. doi: 10.1029/2005JA011315

Zhang, X. X., Wang, C., Chen, T., Wang, Y. L., Tan, A., Wu, T. S., ... Wang, W. (2005). Global patterns of Joule heating in the high-latitude ionosphere. *J. Geophys. Res.*, *110*(A12), A12208. doi: 10.1029/2005JA011222

Zhu, Q., Deng, Y., Richmond, A., & Maute, A. (2018). Small-Scale and Mesoscale Variabilities in the Electric Field and Particle Precipitation and Their Impacts on Joule Heating. *Journal of Geophysical Research: Space Physics*, *123*(11),

9862–9872. doi: 10.1029/2018JA025771

Zou, S., Lyons, L. R., Nicolls, M. J., Heinselman, C. J., & Mende, S. B. (2009). Nightside ionospheric electrodynamics associated with substorms: PFISR and THEMIS ASI observations. *Journal of Geophysical Research: Space Physics*, *114*(12), 1–24. doi: 10.1029/2009JA014259